Evaluation of Different Models in Rainfall-triggered Landslide Susceptibility Mapping: A Case Study in Chunan, Southeast China

Hangjian Feng[1,3], Jianjun Yu[2*], Jiali Zheng[4], Xiaoming Tang[3], Chenchuan Peng[1]

1. China University of Geosciences, Wuhan 430074, China;

2. Environmental Change Institute, School of Geography and the Environment, University of Oxford, Dyson Perrins Building, South Parks Road, Oxford OX1 3QY, the UK;

3. Zhejiang Institute of Geology and Mineral Resources, Hangzhou 310007, China;

4. School of Earth Sciences, Zhejiang University, Hangzhou 310027, China

***Correspondence:** Dr. Jianjun Yu, Environmental Change Institute, School of Geography and the Environment, University of Oxford, Dyson Perrins Building, South Parks Road, Oxford OX1 3QY, the UK; Tel: +44 (0)1865 285070, Fax: +44 (0)1865 275885; E-mail: yujianjun0011@gmail.com

Abstract:

This study applied the information value model (IVM), logistic regression (LR), artificial neural networks (ANN) and support vector machine (SVM) to rainfall-triggered landslide susceptibility mapping for a typical study area in southeast China. Their capabilities under 42 modelling scenarios with different combination of 9 conditioning factors were tested and compared using the performance metric of area under receiver operating characteristic curve (AUC). The results showed that all the models could acceptably produce landslide susceptibility maps (LSMs) with the achieved AUC of 86.05%, 85.89%, 87.65% and 85.63% for model training, and that of 86.03%, 85.7%, 86.4% and 85.11% for model validation. Slightly, ANN was best, followed by LR, IVM and SVM. The LR showed a better generalization capability under the circumstances of changing combination of the conditioning factors, whereas the performance of ANN and SVM appeared to be sensitive to that. Although the comparable performance (i.e. AUC) could be achieved by all the models, the hazard zones classified from the produced LSMs exhibited considerable variation in spatial patterns. The IVM tended to overestimate the landslide susceptibility compared to others, and predicted a less area at very low-level hazard. The associated uncertainty caused by the modelling methods will lead to different management costs and risks being taken when applying the produced LSMs in geological engineering design and planning.

Keywords: Southeast China, landslide susceptibility, rainfall triggered, information value, artificial neural networks, uncertainty

1. INTRODUCTION

The rainfall-triggered landslide has posed an extensive threat to human lives and regional economics due to the increasing rainfall extremes and expansion of settlements to landslide-prone areas (Guzzetti et al., 1999). It is one of the most destructive natural hazards in southeast China where the heavy (from August to September) or prolonged rainfall (from May to July) is the triggering factor. For example in Zhejiang province, China, totally 2,808 landslides have occurred in the period from 2011 to 2015. They have caused 36 casualties and direct economic loss of 0.28 billion Chinese RMB (Zhejiang Provincial Department of Land Resources, 2015). The landslide susceptibility mapping indicates the spatial proneness of the ground to landslides taking the influence of terrain, geologic and geomorphologic factors into consideration (Guzzetti et al., 2012). It provides the essential scientific information for risk assessment and geological engineering design (Fell et al., 2008; van Westen et al., 2008).

Over the past decades, numerous methods for landslide susceptibility mapping have been reported. Examples of them include physical-based models (Casadei et al., 2003; Goetz et al., 2011; Lian et al., 2014), semi-expert models (e.g. analytical hierarchy process and weighted linear combination) (Ayalew et al., 2004; Kayastha et al., 2013), statistical models (e.g. logistic regression, LR) (Dai and Lee, 2003; Ayalew and Yamagishi, 2005; Bhandary et al., 2013; Xu et al., 2013), weight of evidence model (Armaş, 2012; Pourghasemi et al., 2012; Jaafari et al., 2014; Sharma et al., 2015), and various artificial intelligent models such as

artificial neural networks (ANN) (Lee et al., 2004; Gomez and Kavzoglu, 2005; Ermini et al., 2005; Pradhan and Lee, 2010b), neuro-fuzzy system (Vahidnia et al., 2010; Sezer et al., 2011) and support vector machine (SVM) (Yao et al., 2008; Xu et al., 2012a). Whilst the explosion of the models tested for landslide susceptibility mapping, a number of comparison studies have also investigated their capabilities in addressing the same problem (Ayalew et al., 2005; Rozos et al., 2011; Akgun, 2012; Choi J., et al., 2012; Schicker and Moon, 2012; Xu et al., 2012b; Demir et al., 2013; Michel et al., 2014; Regmi et al., 2014).

The data-driven-based modelling approaches have some common characteristics including (i) to establish the relationship between geo-environmental variables (e.g. topography, lithology and land cover etc.) and observed landslides and in some cases including stable slopes as well; and (ii) to infer the probability of landslide occurrence across the study area (Guzzetti et al., 2005). However, there is no agreement on the best model and the most appropriate approach for landslide susceptibility mapping in a specific study case. In addition, the impact of the selected models on the produced landslide susceptibility maps (LSMs) is of particular importance in practical applications (e.g. land use planning, infrastructure design and early warning) (Fell et al., 2008; Hart and Hearn, 2013; Lian et al, 2013; Wu et al., 2014). Practically, the area under receiver operating characteristic curve (AUC) is normally used to evaluate the accuracy of landslide susceptibility mapping. Nevertheless, small difference of the AUC might lead to significant variation (e.g. appearance) in the produced LSMs (Goetz et al., 2011; Goetz et al., 2015). In order to achieve robustness in practices, it is necessary to understand and be aware of the uncertainty associated in the LSMs produced by various

88 modelling approaches.

89

90 Specifically in China, many literatures have reported the development of LSMs in the
91 northwest and southwest regions (Zhao et al., 2015; Wu et al., 2016) where the earthquakes
92 are the major triggering factors. However, the studies regarding the southeast China are still
93 limited, where the landslides are characterized by small magnitudes, rainfall domination, and
94 intensive anthropogenic interference. Therefore, the objective of this study is to develop
95 LSMs for Chunan, southeast China using widely adopted models including information value
96 model (IVM), LR, ANN and SVM. Totally 42 modelling scenarios with different
97 combination of 9 conditioning factors will be tested for the best practices in rainfall-triggered
98 landslide susceptibility mapping and find out the most suitable model for this reported study
99 area. The difference in terms of the spatial pattern of the classified hazard zone maps will be
100 further investigated to gain the awareness of the inherent uncertainty caused by the selected
101 models.

102 2. STUDY CASE AND MATERIALS

103 2.1 Study Area

104 The study area is located in Chunan county, Zhejiang province, southeast China, covering a
105 region between latitude 29°11' N and 30°02' N, and longitude 118°20' E and 119°20' E (Fig.
106 1). It has an area of 4,427 km^2, out of which, 537 km^2 is covered by Xinanjiang reservoir (i.e.
107 water body). The elevation ranges from 108 to 1,527 m. This study area is characterized by a

subtropical climate, with an annual mean temperature of 17.2°C. The monthly mean temperature ranges from 5.2°C in winter to 28.6°C in summer. Historically, the amount of annual precipitation varies from 1,025 to 2,111 mm with an average of 1,478 mm. The average number of raining days is 175. The high-intensity storms occur majorly in June and July. From Fig. 2, the monthly average numbers (over a period from 1990 to 2013) of storms and landslides show a positive correlation. The number of storm days and landslides reach to the peak in June simultaneously, and decrease rapidly before and after it. It shows that high-intensity rainfall is the most important triggering factor of the landslides in this study area.

Place Figures 1 and 2 here

2.2 Landslide Inventory Map

Mapping of the existing landslides is a prerequisite for causative factor analysis and susceptibility mapping. The landslide inventory records the spatial location of the landslides with corresponding features including type, magnitude and time of occurrence etc. This study area is covered by dense vegetation but the magnitude of the landslides is low. Because of this, it is difficult to interpret existing landslides directly from remote sensing images. Hence, we initially delineated the unstable slopes by visual interpretation from a colour aerial image (with horizontal resolution of 0.5 m). The detailed field surveys were then carried out in the delineated region to identify the landslides (Feng et al., 2014). From Fig. 1, there are totally

596 landslides occurring in the period from 1990 to 2013. The major landslide types are rock landslide and soil landslide. Those shallow soil landslides account for 89.5% of all ones. A majority of landslides (i.e. 580) have a low magnitude less than 1,000 m^2, and the average volume of these landslides are 6,000 m^3. The sliding distance is averagely between 5 and 20 m. The material composition of soil landslide is mainly el-dlQ which includes pebbly clay and completely and heavily weathered rock formation such as mud rock.

2.3 Thematic Layers and Data Preparation

Table 1 lists totally 9 potential conditioning factors and corresponding categories considered in this study. These conditioning factors could be classified into three groups which reflect the influences of topography (i.e. elevation, slope, aspect, curvature and distance to drainage), geology (i.e. lithology and distance to fault) and anthropogenic activity (i.e. land use and distance to road), respectively. Fig. 3 shows the correlation of landslide point density (LPD, denoted as the number of landslides per 10 km^2) and area percentage of each category of the 9 conditioning factors. The ArcGIS 10 software (ESRI, 2011) is used for data process and thematic layer preparation. All of the vector thematic layers are converted to raster maps with 10 m resolution. Each pixel is then reclassified into specific category according to the criteria listed in Table 1.

Place Table 1 and Figure 3 here

The digital elevation model (DEM) in a horizontal resolution of 10 m is interpolated from a contour map with a scale of 1:10,000. The DEM is subsequently used to derive slope, aspect and curvature layers considering these geomorphologic and topographic factors are contributed to slope instability. As shown in Figs. 3a and 3b, a large number of landslides occur in the areas with the elevation from 100 to 200 m and slope from 10° to 30°, where the intensive human activities (e.g. construction) remarkably affect the slope stability. The sufficient amounts of rainfall and sunshine in south and southeast facing slopes result in much erosion leading to slope instability (Fig. 3c). A buffer zone map with 50-m interval to the drainage is created to consider the influence of the dense river network.

Lithology is widely recognized as one of the most important conditioning factors causing different susceptibility degrees (Ayalew and Yamagishi, 2005). In order to provide sufficient information on rock composition and rock mass strength, the stratigraphic legends of a geological map with a scale of 1:50,000 are converted to engineering geological classifications (Carrara et al., 1999; van Westen et al., 2008). Fig. 4 shows the derived lithology map having 11 lithology types (please refer to Table 2 for corresponding description of geologic units). The lithology type of Sf, Tcc and SRc are susceptible to landslides (Fig. 3f) because of the corresponding rock types give weak resistance to driving forces. Structurally, the landslides are prone to occur in the areas close to (within 100 m) the geological faults (Fig. 3g). A buffer zone map with 50-m interval to the faults is created to reflect different levels of structural tectonic feature influence.

Finally, intensive anthropogenic activities (e.g. land use change and construction) are also considered to have considerable influences on slope stability. For example in Fig. 3h, higher LPD is observed in human interfered residential land. A polygon layer with 10 land use types is digitized from a 0.5 m resolution colour aerial photo. In addition, a buffer zone map with 60-m interval to the road is also created to consider the instability of artificial cut slopes.

Place Table 2 and Figure 4 here

---

3. METHODOLOGIES

IVM employs information value (i.e. a ratio of relative frequency) to represent the likelihood of landslide occurrence conditioned on the existing landslides. The information value (I_{ij}) could be calculated for category *j* of conditioning factor *i* as follows:

$$I_{ij} = \ln \frac{N_j/N}{S_j/S} \quad (1)$$

where N_j and N denotes the number of grids classified as category *j* and total number of grids having landslides occurred, respectively; S_j denotes the total number of grids classified as category *j*; and *S* denotes the total number of grids across the study area. The total information value (*I*) of a grid is calculated by summation of I_{ij}:

$$I = \sum_{i=1}^{n} I_{ij} \quad (2)$$

where *n* is the number of conditioning factors; and *j* is the index of the category the concerned grid is classified as. Table 3 lists the information values of all the categories of the 9 conditioning factors.

193 ----------

194 Place Table 3 here

195 ----------

196

197 LR is a multivariate statistical model suitable for approximating the relationship between
198 independent variables and binary or dichotomous output. In using LR, the probability (p) of
199 landslide occurrence is written as:

200 $$p = \frac{1}{1+e^{-y}} \quad (3a)$$

201 $$y = \sum_{i=1}^{n} b_i x_i + b_0 \quad (3b)$$

202 where n is the number of conditioning factors; x_i is the information value of the category of
203 ith conditioning factor as which the concerned grid is classified; and b_i is regression
204 coefficient under estimation.

205

206 The ANN, analogue to human neural system, consists of neurons settled in multiple layers
207 and connected by weighted links. It is capable of approximating nonlinear relationship whilst
208 has many advantages like fast convergence, handling of imprecise and fuzzy data, and
209 avoiding over-fitting (Pradhan, et al., 2010). These characteristics enable ANN as an
210 alternative to statistical regressions for data fitting problems. In order to solve the formulated
211 problem, it is essential to determine the fundamental components of the neural networks
212 including (i) network architecture; (ii) the number of hidden layers and neurons; (iii) transfer
213 function; and (iv) learning algorithm and associated settings etc. Referring to many studies
214 applying ANN for landslide susceptibility mapping (Ermini et al., 2005; Pradhan and Lee,

2010; Choi et al., 2012), the feed-forward neural network (FFNN), characterized as neuron connections orientated from input towards output only, is selected in this study due to its easy-to-implementation. The three layers neural network with only one hidden layer settled with 11 neurons is determined. The sigmoid function is used as transfer function in each neuron. The FFNN is trained by back-propagation algorithm with learning rate set to 0.7. The training will stop until the minimal standard error or the maximum number of iterations (i.e. 2,000) is reached. A trial-and-error is used to determine the initial weights of the neurons. According to the AUC, the model with best performance from a couple of runs is selected to predict the susceptibility value across the study area. The strategy of creating training and validation datasets is same for LR, ANN and SVM, which is described in the following sections.

SVM is a supervised machine learning model for solving classification or regression problems based on a best hyperplane in a high-dimensional space through maximizing the functional margin (Cortes and Vapnik, 1995). Given training data points $\mathbf{x}_i$ along with their class label y_i (+1 or -1 standing for landslide and stable slope location in landslide susceptibility mapping), to find the best hyperplane is equivalent to find the optimal solution of $\mathbf{w}$ and b to minimize $\|\mathbf{w}\|$ such that for all training data points $(\mathbf{x}_i, y_i)$ satisfying the following equation:

$$y_i(\mathbf{w}\mathbf{x}_i + b) \geq 1 \quad (4)$$

where $\|\mathbf{w}\|$ is the norm of the hyperplane and b is a scalar real number. Mathematically, through introducing positive Lagrange multipliers α_i, minimizing the following equation

could lead to solution of **w** and *b*:

$$\frac{1}{2}\|\mathbf{w}\|^2 - \sum_{i=1}^{n} \alpha_i (y_i(\mathbf{w}\mathbf{x}_i + b) - 1) \quad (5)$$

In the case of non-separable data, SVM tries to find a soft margin to make the hyperplane separate many but not all of the data points. A penalty term is introduced to achieve the trade-off between a stricter separation and misclassification. Accordingly, the objective function could be written as:

$$\frac{1}{2}\|\mathbf{w}\|^2 + C\sum_{i=1}^{n} s_i \quad (6a)$$

subject to:

$$y_i(\mathbf{w}\mathbf{x}_i + b) \geq 1 - s_i \quad (6b)$$

$$s_i \geq 0 \quad (6c)$$

where s_i is the slack variable and *C* is a penalty parameter. In applying to landslide susceptibility mapping, we introduced the Gaussian kernel function $K(\mathbf{x}_i, \mathbf{x}_j)$ to obtain a nonlinear classifier, which could be written as:

$$K(\mathbf{x}_i, \mathbf{x}_j) = e^{-\frac{\|\mathbf{x}_i - \mathbf{x}_j\|^2}{2\sigma^2}} \quad (7)$$

where σ is the correlation length. In model training, the optimal values of *C* and σ are determined by a 5-folder cross-validation procedure. This is implemented by an iterative grid search algorithm to find the optimal values from a sampling space of -512 to 512 with the searching step of 0.01 (Chang and Lin 2011).

Different from the IVM considering only the positive samples (i.e. landslides), the LR, ANN and SVM models need both positive and negative samples (i.e. stable slopes). Totally 451 landslides (i.e. 75%) out of 596 are randomly selected as positive samples meanwhile 451

negative samples are selected from stable slopes randomly for model training (Fig. 1). The strategy of using same number of positive and negative samples for model training is widely adopted in order to avoid the bias caused by unequal proportions of landslide and non-landslide pixels (Yeşilnacar and Topal, 2005; Tien Bui et al.; 2011, Xu et al., 2012b). The information values of the concerned grid (look up Tables 1 and 3) are used to feed the models. The established models are verified by AUC using the rest 145 (i.e. 25%) landslides (Fig. 1). The acceptable models are then applied to infer the landslide probability across the whole study area to produce LSMs. Subsequently, the LSM is classified into four levels of hazard zones (i.e. denoted as high, moderate, low, and very low) according to natural breaks method (Ayalew et al., 2004).

4. RESULTS OF ANALYSIS

Table 4 lists the AUC of landslide susceptibility mapping in using IVM, LR, ANN and SVM for 42 scenarios under the changing combination of 9 conditioning factors. These scenarios are selected from all the possible combinations according to the criteria of (i) including minimum 5 conditioning factors; (ii) avoiding dependence between pairs of conditioning factors by chi-square test (Lee and Choi, 2010); (iii) reflecting all the influences of topography, geology and anthropogenic activities (i.e. including at least one conditioning factor belonging to each group). All the models perform best in training when using 7 conditioning factors of elevation, slope, aspect, curvature, distance to drainage, lithology and land use (i.e. NO. 41 in Table 4) as model inputs. The achieved AUC is 86.05%, 87.65%, 85.89% and 85.63% for IVM, LR, ANN and SVM, respectively. The ANN slightly outperforms others in model training under the circumstance of using same conditioning

281 factors, whereas its performance is sensitive to the changing combination of conditioning
282 factors (and so is SVM). The LR performs best in model validation in most cases, which is
283 slightly better than IVM. However, it should be noted that the performance of LR is easily to
284 be affected by the value (representing the category of each conditioning factor) used for
285 model training. Using the information value instead of category integer for model training as
286 did in this study could improve the model performance of LR significantly. The consistent
287 conclusion and details could also be referred to Ayalew and Yamagishi (2005) and Greco et
288 al. (2007). The ANN and SVM are more robust than LR to handle the potential data noise.

289 ----------

290 Place Table 4 here

291 ----------

292 Figs. 5a and 5b show the variation of AUC in model training and validation under different
293 conditioning factor combinations. It is surprisingly that all the models perform relatively
294 worse (i.e. at lower whiskers with AUC lower than 75%) when the conditioning factor of
295 distance to road is considered. It is identified as a major causative factor of landslides from
296 expert knowledge perspective since the road construction will cause instable artificial slope
297 cut. However, the existing landslides (i.e. samples for model training) in road construction
298 affected areas are still less in that they only occurred recently along with the economic
299 growth in southeast China. It therefore results in inaccurate model fitting mathematically. If
300 these modelling scenarios are not taken into consideration, all the models show a similar level
301 of uncertainty with the AUC varying from around 80% to 87% in both model training and
302 validation. The results render that there is no agreement on which model is the best in terms
303 of AUC amongst IVM, LR, ANN and SVM. Fig. 5c shows the prediction rate curve of the
304 optimum models (i.e. NO. 41 in Table 4), which are capable of achieving highest AUC in
305 model training. Although the prediction accuracy of all the models (i.e. with the AUC of

306 86.03%, 86.4%, 85.7% and 85.11%) is not the best under this modelling scenario, such a
307 model configuration could consider diverse conditioning factors from expert knowledge
308 perspective and thus is selected for further analysis.

309 ----------

310 Place Figure 5 here

311 ----------

312 Fig. 6 shows the variation of area percentages of the hazard zones classified from LSMs
313 produced by the 42 models. They show a similar level of variation from around 10% to 35%
314 in high-level hazard zones (Fig. 6d). On the contrast, from Fig. 6a, the classified very
315 low-level hazard zones exhibit remarkable difference. The area percentage is averagely 12%
316 (varying from 8% to 18%) in applying IVM, which is particularly lower than those of 29%
317 (varying from 18% to 38%), 22% (varying from 5% to 32%) and 43% (varying from 18% to
318 62%) in using LR, ANN and SVM, respectively. It implies that IVM tends to overestimate
319 the risk of landslide occurrence compared to others and thus will result in the classified very
320 low-level hazard zone having smaller area. Overall, the variation of AUC is moderate under
321 various modelling scenarios whereas the classified hazard zone maps exhibit a large
322 uncertainty (Goetz et al., 2011; 2015). Specifically, the emphasis should go to very low-level
323 hazard zone when applying the classified hazard maps in practices (e.g. safety construction
324 siting purpose).

325 ----------

326 Place Figure 6 here

327 ----------

328

329 Fig. 7 illustrates the hazard zone maps classified from LSMs produced by IVM, LR, ANN
330 and SVM. They demonstrate obvious differences in appearance and spatial pattern of the

hazard zones. It appears that the hazard zone map produced by IVM indicates more regions with high-level hazard, and that from LR identifies more very-low-level zones. Figs. 8a-8d show the distribution of the predicted landslide susceptibility values. A large percentage of grids (i.e. 44.7%) are predicted at a median range (i.e. from 0.4 to 0.6) of the susceptibility values by IVM. The susceptibility values predicted by LR have 65.7% distributed in the range below than 0.4. Those predicted by ANN and SVM show a similar characteristic with approximate 60% of the value in the range from 0.25 to 0.5. Although a comparable AUC (i.e. 85% to 86%) is achieved by these models, the different distribution characteristics of the inferred susceptibility values will lead to the variation of the classified hazard zone maps and eventually affect the decision making.

From Figs. 8e-8h, a similar percentage (i.e. approximately 15% -19%) of the area is classified as high level hazard zone. However, the difference in very-low- and low-level hazard zone is remarkable. Around 40% of the area is classified as very-low-level hazard zone in applying LR and SVM. The IVM appears to overestimate the landslide susceptibility resulting in only 13% of very low-level hazard zone. This will considerably restrict the available locations for spatial siting in engineering planning (e.g. land use planning for settlement) practically. Figs 8i to 8p illustrate the spatial patterns of high- and very low-level hazard zones produced by different models, in which the rose maps show the distribution of area percentage at various directions geographically. The high-level hazard zone produced by IVM indicates slightly higher landslide risk in all directions than other models. However from Fig. 8m, the north-west regions are not identified as very-low risk region. Consequently, due to the spatial heterogeneity in the produced hazard zone maps, in applying them for geological engineering design and planning will potentially lead to different management costs (e.g. over-investment to avoid infrastructures being located at high-level hazard zones) and risks being taken (e.g.

356 damage caused by landslide due to underestimation of the risk).

357 ----------

358 Place Figures 7 and 8 here

359 ----------

360 5. DISCUSSIONS AND CONCLUSIONS

361 This study applied 4 widely acknowledged models including information value model (IVM),
362 logistic regression (LR), artificial neural networks (ANN) and support vector machine (SVM)
363 to landslide susceptibility mapping under totally 42 modelling scenarios with different
364 combination of 9 conditioning factors. A typical case study in Chunan, southeast China was
365 selected for demonstration, where the heavy and prolonged rainfall triggers the hazards.
366 Firstly, there is no agreement on the best model for this study case. All the models tested
367 herein could achieve an acceptable AUC of 86% for both model training and validation.
368 Slightly, ANN is the best, followed by LR, IVM and SVM. The LR shows relatively better
369 generalization capability in model validation, whereas the performance of ANN and SVM is
370 sensitive to the changing combination of conditioning factors. It suggests that extensive
371 trial-and-error of different conditioning factors is necessary to find out the optimum and to be
372 aware of the potential uncertainty. Nevertheless, the performance of LR is easy to be affected
373 by the values representing conditioning factors used as model input for training. Employment
374 of information value instead of ordinary numbers as model input will improve LR model
375 performance.

376

377 Secondly, AUC is widely adopted as the metric for evaluating the accuracy of landslide
378 susceptibility mapping (Yeşilnacar and Topal, 2005). The threshold for selecting an

acceptable model is normally determined subjectively. As shown in this study, a small variation of AUC will lead to significant differences in not only the distributions of the inferred landslide susceptibility values but also the spatial patterns of the classified hazard zone maps, in particular, in very low-level hazard zones. The IVM tends to overestimate the landslide susceptibility to indicate a slightly higher risk across the study area. Particularly, the area percentage of the classified very low-level hazard zones is only 14%, which is much lower than that of 40% in using LR and SVM. It implies that AUC is capable of facilitating model comparison in the sense of identifying high risk areas prone to landslide, but to some extent is misleading for low risk areas. Therefore, the associated uncertainty in low risk areas caused by different models applied to landslide susceptibility mapping should be concerned.

Finally, there existed a lot of uncertainty sources throughout the landslide susceptibility mapping process, for instances the sampling strategy, resolution of modelling grids and discretization of continuous values etc. They will unavoidably lead to spatial heterogeneity of the produced landslide susceptibility maps and eventually cause different management costs and risks being taken in practices. Further research is thus desired to develop a holistic modelling framework to quantify the uncertainty in landslide susceptibility mapping. As an attempt, understanding the advantage and disadvantage of various modelling methods and awareness of uncertainty is valuable for best practices of applying produced landslide susceptibility maps to risk-based engineering design and decision making.

ACKNOWLEDGEMENT

The research work was partly supported by the public welfare technology application research project of Zhejiang province, China (No.2016C33045). The authors also deeply appreciate Mr. Shengyi You, Mrs. Xueqin Wu and Mr. Zhong Zhang in Zhejiang Institute of

403 Geology and Mineral Resources for the filed survey work.

404 REFERENCES

405 Akgun A., 2012. A comparison of landslide susceptibility maps produced by logistic
406 regression, multi-criteria decision, and likelihood ratio methods: a case study at İzmir,
407 Turkey. Landslides 9, 93-106.

408 Armaş I ., 2012. Weights of evidence method for landslide susceptibility mapping. Prahova
409 Subcarpathians, Romania. Natural Hazards 60, 937-950.

410 Ayalew L., Yamagishi H., Ugawa N., 2004. Landslide susceptibility mapping using
411 GIS-based weighted linear combination, the case in Tsugawa area of Agano River,
412 Niigata Prefecture, Japan. Landslides 1, 73-81.

413 Ayalew L., Yamagishi H., 2005. The application of GIS-based logistic regression for
414 landslide susceptibility mapping in the Kakuda-Yahiko Mountains, Central Japan.
415 Geomorphology 65, 15-31.

416 Ayalew L., Yamagishi H., Marui H., Kanno T., 2005. Landslides in Sado Island of Japan: Part
417 II. GIS-based susceptibility mapping with comparisons of results from two methods and
418 verifications. Engineering Geology 81, 432-445.

419 Bhandary N.P., Dahal R.K., Timilsina M., Yatabe R., 2013. Rainfall event-based landslide
420 susceptibility zonation mapping. Natural Hazards 69, 365-388.

421 Carrara A., Guzzetti F., Cardinali M., Reichenbach P., 1999. Use of GIS Technology in the
422 Prediction and Monitoring of Landslide Hazard. Natural Hazards 20, 117 - 135.

423 Casadei M., Dietrich W.E., Miller N.L., 2003. Testing a model for predicting the timing and

location of shallow landslide initiation in soil-mantled landscapes. Earth Surface Processes and Landforms 28, 925-950.

Chang CC., Lin CJ., 2011. LIBSVM: a library for support vector machines. ACM Trans Intell Syst Technol (TIST), 2(3):27.

Choi J., Oh H.J., Lee H.J., Lee C., Lee S., 2012. Combining landslide susceptibility maps obtained from frequency ratio, logistic regression, and artificial neural network models using ASTER images and GIS. Engineering Geology 124, 12-23.

Cortes C., Vapnik V., 1995. Support-vector networks. Machine learning 20, 273-297.

Dai F.C., Lee C.F., 2003. A spatiotemporal probabilistic modelling of storm‐induced shallow landsliding using aerial photographs and logistic regression. Earth Surface Processes and Landforms 28, 527-545.

Demir G., Aytekin M., Akgün A., İkizler S.B., Tatar O., 2013. A comparison of landslide susceptibility mapping of the eastern part of the North Anatolian Fault Zone (Turkey) by likelihood-frequency ratio and analytic hierarchy process methods. Natural Hazards 65, 1481-1506.

Ermini L., Catani F., Casagli N., 2005. Artificial neural networks applied to landslide susceptibility assessment. Geomorphology 66, 327-343.

Esri, A. D., 2011. Release 10. Documentation Manual. Redlands, CA, Environmental Systems Research Institute.

Fell R., Corominas J., Bonnard C., Cascini L., Leroi E., Savage W.Z., 2008. Guidelines for landslide susceptibility, hazard and risk zoning for land use planning. Engineering Geology 102, 85-98.

Feng H.J., Zhou A.G.,Tang X.M., Yu J.J., 2014. Study on Remote Sensing Interpretation for Implicit Geohazard in Southeast China. Geological Review 60, 1370-1380. (in Chinese).

Gomez H., Kavzoglu T., 2005. Assessment of shallow landslide susceptibility using artificial neural networks in Jabonosa River Basin, Venezuela. Engineering Geology 78, 11-27.

Goetz J.N., Guthrie R.H., Brenning A., 2011. Integrating physical and empirical landslide susceptibility models using generalized additive models. Geomorphology 129, 376-386.

Goetz J.N., Brenning A., Petschko H., Leopold P., 2015. Evaluating machine learning and statistical prediction techniques for landslide susceptibility modeling. Computers & Geosciences 81, 1-11.

Greco R., Sorriso-Valvo M. , Catalano E., 2007. Logistic Regression analysis in the evaluation of mass movements susceptibility: The Aspromonte case study, Calabria, Italy. Engineering Geology 89, 47-66.

Guzzetti F., Carrara A., Cardinali M., Reichenbach P., 1999. Landslide hazard evaluation: a review of current techniques and their application in a multi-scale study, Central Italy. Geomorphology 31, 181 - 216.

Guzzetti F., Reichenbach P., Cardinali M., Galli M., Ardizzone F., 2005. Probabilistic landslide hazard assessment at the basin scale. Geomorphology 72, 272-299.

Guzzetti F, Mondini AC, Cardinali M, Fiorucci F, Santangelo M, Chang K (2012) Landslide inventory maps: New tools for an old problem. Earth Sciences Review 112(1-2):42-66.

Hart A.B., Hearn G.J., 2013. Landslide assessment for land use planning and infrastructure management in the Paphos District of Cyprus. Bulletin of Engineering Geology and the Environment 72, 173-188.

Jaafari A., Najafi A., Pourghasemi H.R., Rezaeian J., Sattarian A., 2014. GIS-based frequency ratio and index of entropy models for landslide susceptibility assessment in the Caspian forest, northern Iran. International Journal of Environmental Science and Technology 11, 909-926.

Kayastha P., Dhital M.R., De Smedt F., 2013. Application of the analytical hierarchy process (AHP) for landslide susceptibility mapping: a case study from the Tinau watershed, west Nepal. Computers & Geosciences 52, 398-408.

Lee S., Ryu J.H., Won J.S., Park H.J., 2004. Determination and application of the weights for landslide susceptibility mapping using an artificial neural network. Engineering Geology 71, 289-302.

Lee S., Choi J., 2010. Landslide susceptibility mapping using GIS and the weight-of-evidence model. International Journal of Geographic Information Science 18(8), 789-814.

Lian C., Zeng Z., Yao W., Tang H., 2013. Displacement prediction model of landslide based on a modified ensemble empirical mode decomposition and extreme learning machine. Natural Hazards, 66, 759-771.

Lian C., Zeng Z., Yao W., Tang H., 2014. Ensemble of extreme learning machine for landslide displacement prediction based on time series analysis. Neural Computing and Applications 24, 99-107.

Michel G.P., Kobiyama M., Goerl R.F., 2014. Comparative analysis of SHALSTAB and SINMAP for landslide susceptibility mapping in the Cunha River basin, southern Brazil. Journal of Soils and Sediments 14, 1266-1277.

490 Pradhan B., Lee S., 2010. Regional landslide susceptibility analysis using back- propagation
491 neural networks model at Cameron Highland, Malaysia. Landslides 7(1), 13–30.
492 Pradhan, B., Youssef, A.M., Varathrajoo, R., 2010. Approaches for delineating landslide
493 hazard areas using different training sites in an advanced artificial neural networks model.
494 Geo-spatial Information Science 13 (2), 93–102.
495 Pourghasemi H.R., Mohammady M., Pradhan B., 2012. Landslide susceptibility mapping
496 using index of entropy and conditional probability models in GIS: Safarood Basin, Iran.
497 Catena 97, 71-84.
498 Regmi A.D., Devkota K.C., Yoshida K., Pradhan B., Pourghasemi H.R., Kumamoto T.,
499 Akgun A., 2014. Application of frequency ratio, statistical index, and
500 weights-of-evidence models and their comparison in landslide susceptibility mapping in
501 Central Nepal Himalaya. Arabian Journal of Geosciences 7, 725-742.
502 Rozos D., Bathrellos G.D., Skillodimou H.D., 2011. Comparison of the implementation of
503 rock engineering system and analytic hierarchy process methods, upon landslide
504 susceptibility mapping, using GIS: a case study from the Eastern Achaia County of
505 Peloponnesus, Greece. Environmental Earth Sciences 63, 49-63.
506 Schicker R., Moon V., 2012. Comparison of bivariate and multivariate statistical approaches
507 in landslide susceptibility mapping at a regional scale. Geomorphology 161, 40-57.
508 Sezer E.A., Pradhan B., Gokceoglu C., 2011. Manifestation of an adaptive neuro-fuzzy model
509 on landslide susceptibility mapping: Klang valley, Malaysia. Expert Systems with
510 Applications 38, 8208-8219.
511 Sharma L.P., Patel N., Ghose M.K., Debnath P., 2015. Development and application of

512 Shannon's entropy integrated information value model for landslide susceptibility
513 assessment and zonation in Sikkim Himalayas in India. Natural Hazards 75, 1555-1576.
514 Tien Bui, D., Lofman, O., Revhaug, I., Dick, O., 2011. Landslide susceptibility analysis in
515 the Hoa Binh province of Vietnam using statistical index and logistic regression. Natural
516 Hazards 59(3), 1413-1444.
517 Vahidnia M.H., Alesheikh A.A., Alimohammadi A., Hosseinali F., 2010. A GIS-based
518 neuro-fuzzy procedure for integrating knowledge and data in landslide susceptibility
519 mapping. Computers & Geosciences 36, 1101-1114.
520 van Westen C.J., Castellanos E., Kuriakose S.L., 2008. Spatial data for landslide
521 susceptibility, hazard, and vulnerability assessment: An overview. Engineering Geology
522 102, 112-131.
523 Wu Y., Chen L., Cheng C., Yin K., Török Á., 2014. GIS-based landslide hazard predicting
524 system and its real-time test during a typhoon, Zhejiang Province, Southeast China.
525 Engineering Geology 175, 9-21.
526 Wu Y., Li W., Wang Q., Liu Q., Yang Q., Xing M., Pei Y., Yan S., 2016 Landslide
527 susceptibility assessment using frequency ratio, statistical index and certainty factor
528 models for the Gangu County, China. Arabian Journal of Geosciences 9(2), 1-16.
529 Xu C., Dai F., Xu X., Lee Y.L., 2012a. GIS-based support vector machine modeling of
530 earthquake-triggered landslide susceptibility in the Jianjiang River watershed, China.
531 Geomorphology 145-146, 70-80.
532 Xu C., Xu X., Dai F., Saraf A.K., 2012b. Comparison of different models for susceptibility
533 mapping of earthquake triggered landslides related with the 2008 Wenchuan earthquake

534 in China. Computers & Geosciences 46, 317-329.
535 Xu C., Xu X., Dai F., Wu Z., He H., Shi F., Wu X., Xu S., 2013. Application of an incomplete
536 landslide inventory, logistic regression model and its validation for landslide
537 susceptibility mapping related to the May 12, 2008 Wenchuan earthquake of China.
538 Natural Hazards 68, 883-900.
539 Yao X., Tham L.G., Dai F.C., 2008. Landslide susceptibility mapping based on support vector
540 machine: a case study on natural slopes of Hong Kong, China. Geomorphology 101,
541 572–582.
542 Yeşilnacar E.K., Topal T., 2005, Landslide Susceptibility Mapping: comparison between
543 logistic regression and neural networks in a medium scale study, Hendek region
544 (TURKEY), Engineering Geology 79 (3-4), 251-266.
545 Zhao C., hen W., Wang Q., Wu Y., Yang B., 2015 A comparative study of statistical index and
546 certainty factor models in landslide susceptibility mapping: a case study for the
547 Shangzhou District, Shaanxi Province, China. Arabian Journal of Geosciences 8 (11),
548 9079-9088.
549 Zhejiang Provincial Department of Land Resources, 2015, Bulletin of Zhejiang geological
550 environment: 2011-2015 (Internal report in Chinese).
551

Table Caption List:

Table 1. Conditioning factors and their categories.

Table 2. Description of lithology and geologic units.

Table 3. Information value of various categories of conditioning factors

Table 4. Performance of models under different combination of conditioning factors in using IVM, ANN, LR and SVM

561 **Table 1**.Conditioning factors and their categories

Conditioning factors	*Number of categories*	*Categories*
Elevation (m)	11	(1) <100; (2) 100~200; (3) 200~300; (4) 300~400; (5) 400~500; (6) 500~600; (7) 600~700; (8) 700~800; (9) 800~900; (10) 900~1,000; (11) >1,000
Slope (°)	12	(1) <5; (2) 5~10; (3) 10~15; (4) 15~20; (5) 20~25; (6) 25~30; (7) 30~35; (8) 35~40; (9) 40~45; (10) 45~50; (11) 50~55; (12) >55
Aspect	9	(1) Flat; (2) N; (3) NE; (4) E; (5) SE; (6) S; (7) SW; (8) W; (9) NW
Curvature	12	(1) < -10; (2) -10~-8; (3) -8~-6; (4) -6~-4; (5) -4~-2; (6) -2~0; (7) 0~2; (8) 2~4; (9) 4~6; (10) 6~8; (11) 8~10; (12) >10
Distance to drainage (m)	7	(1) <50; (2) 50~100;(3) 100~150;(4) 150~200;(5) 200~250;(6) 250~300;(7) >300
Lithology	11	(1) Bs; (2) Hi; (3) Qd; (4) Qg; (5) Rr; (6) Sc; (7) Sf; (8) SRc; (9) LT; (10) Tc; (11) Tcc
Distance to fault (m)	7	(1) 0~50; (2) 50~100; (3) 100~150; (4) 150~200; (5) 200~250; (6) 250~300; (7) >300
Distance to road (m)	3	(1) highway (0-60m width), village road (0-30m width); (2) highway (60-120m width), village road (30-60m width); (3) others
Landuse	10	(1) cultivated land; (2) garden; (3) forest land; (4) grassland; (5) industrial and mining storage land; (6) residential land; (7) public facilities land; (8) transportation land; (9) water body and facilities; (10) others

562
563
564
565

566 **Table 2.** Description of lithology and geologic units

Code	*Rock type*	*Description of lithology*	*Geologic unit*
Qg	Intrusive rock	Acid rock petrofabric (e.g. hard and massive granite)	$\xi\gamma_5^2$, γ_5^2, γπ, γ, J_3Hηγ, Pt_3Fγπ, Pt_3 Tγπ, Pt_3Nγ, βμ
Qd		Neutral rock petrofabric (e.g. hard and massive diorite)	απPt_3,γδ, δ, δo, γδπ, δμ, λδμ, J_3 cδσ
Rr	Lava	Hard and massive rhyolite (porphyry) based acid petrofabric	ν, νπ, νοπ, λπ, λπJ_3, λπPT_3
Hi	Pyroclastic rock	Hard medium-thick stratiform and massive tuff rhyolitic porphyry petrofabric	K_1hj, Qb_2S
Bs	Metamorphic rock	Hard, medium-thick stratiform slate and phyllite based metamorphic rock petrofabric	JxP
Sc	Detrital rock	Hard, medium-thick stratiform sandstone and glutenite petrofabric	J_1w, DCz, D_3x, S_2t, NH_2n
Sf		Soft, thin-medium strutiform mudstone (shale) and siltstone petrofabric	C_1y, $S_{1\text{-}2}$k, S_1h, S_1x, O_3w, O_3c, O_3h, O_3y, $O_{2\text{-}3}$h, $O_{1\text{-}2}$n, O_1y, NH_1x, Z_1d, $\in_1$h
SRc		Mixed soft and hard, thin-medium thick seam red sandstone and glutenite petrofabric	K_1h, K_1l, K_1s
Tc	Carbonate rock	Hard, medium thick seam carbonate rocks petrofabric	P_2q, CPc, C_2h, C_2l
Tcc		Hard and stratiform carbonate rocks of clastic rocks	Z_2p, Z_2b, Z_2d, ∈Ox, $\in_3$h, $\in_2$y, $\in_1$d
LT	Loose rock mass	Sandstone and gravel based petrofabric	alQ_4, al-plQ_4

567

568

569

570 **Table 3.** Information value of various categories of conditioning factors

Conditioning factors	*Categories*	N_i	S_i	N_i/S_i	*Information value*
Elevation	1	3	518401	0.000006	-2.76462
	2	231	1062273	0.000217	0.861771
	3	95	839129	0.000113	0.209032
	4	64	732131	0.000087	-0.04956
	5	27	594149	0.000045	-0.70377
	6	19	441129	0.000043	-0.75738
	7	11	291369	0.000038	-0.88918
	8	0	175155	0	-2.76462
	9	0	102379	0	-2.76462
	10	0	63682	0	-2.76462
	11	0	89996	0	-2.76462
Slope	1	4	649253	0.000006	-2.70201
	2	25	214261	0.000117	0.239201
	3	50	278474	0.000180	0.670218
	4	70	379700	0.000184	0.696633
	5	92	516514	0.000178	0.662206
	6	98	662379	0.000148	0.476649
	7	63	791053	0.00008	-0.14271
	8	36	811000	0.000044	-0.72723
	9	13	490467	0.000027	-1.24289
	10	0	104907	0	-2.70201
	11	0	10044	0	-2.70201
	12	0	1741	0	-2.70201
Aspect	1	1	406091	0.000002	-3.61906
	2	16	266020	0.00006	-0.42346
	3	39	561596	0.000069	-0.2797
	4	50	582851	0.000086	-0.06839
	5	86	580341	0.000148	0.478251
	6	75	555983	0.000135	0.38427
	7	53	576948	0.000092	0.000059
	8	62	565253	0.00011	0.177381
	9	47	550622	0.000085	-0.07338
	10	22	264088	0.000083	-0.09772
Curvature	1	0	740	0	-1.49006
	2	1	5856	0.000171	0.620053
	3	0	55147	0	-1.49006
	4	25	256852	0.000097	0.057896
	5	97	692845	0.00014	0.421424
	6	169	1714847	0.000099	0.070339

Controlling factors	*Categories*	N_i	S_i	N_i/S_i	*Information value*
Curvature	7	98	1138253	0.000086	-0.06476
	8	50	724260	0.000069	-0.28561
	9	10	266408	0.000038	-0.89492
	10	1	48307	0.000021	-1.49006
	11	0	5176	0	-1.49006
	12	0	1102	0	-1.49006
Distance to drainage	1	74	610228	0.000121	0.001819
	2	76	569729	0.000133	0.097159
	3	85	531358	0.00016	0.278802
	4	66	489567	0.000135	0.10772
	5	47	441159	0.000107	-0.12767
	6	52	387787	0.000134	0.102374
	7	196	1893929	0.000101	-0.15671
Lithology	1	1	9951	0.000100	-0.0216
	2	8	227272	0.000035	-1.07063
	3	11	15303	0.000719	1.945922
	4	16	165251	0.000097	-0.0588
	5	0	15941	0	-1.31055
	6	18	527209	0.000034	-1.10115
	7	206	2083383	0.000099	-0.0378
	8	41	272694	0.00015	0.381297
	9	2	72224	0.000028	-1.31055
	10	7	48828	0.000143	0.333682
	11	141	953956	0.000148	0.364218
Distance to fault	1	45	258417	0.000174	0.642514
	2	38	257386	0.000148	0.477435
	3	23	251065	0.000092	0.000208
	4	26	239461	0.000109	0.170132
	5	22	224959	0.000098	0.06555
	6	32	210058	0.000152	0.508778
	7	265	3482735	0.000076	-0.18542
Distance to road	1	27	325361	0.000083	-0.10424
	2	20	332924	0.000060	-0.42732
	3	404	4238485	0.000095	0.034317
Landuse	1	27	214837	0.000126	0.313509
	2	95	520529	0.000183	0.686583
	3	188	3436309	0.000055	-0.51816
	4	6	50460	0.000119	0.258131
	5	1	2990	0.000334	1.292279
	6	124	70244	0.001765	2.955859
	7	1	6708	0.000149	0.484251
	8	2	5532	0.000362	1.37015

	9	5	597769	0.000008	-2.39621
	10	2	4574	0.000437	1.560311
	11	27	214837	0.000126	0.313509
	12	95	520529	0.000183	0.686583

571

572 **Notes:** N_i denotes the number of grids classified as the corresponding category where landslides have
573 been observed; and S_i denotes the total number of grids classified as that category.
574

575 **Table 4.** Performance of models under different combination of conditioning factors in using IVM, ANN, LR and SVM

NO	*Conditioning factors*	*Training (AUC %)*				*Validation (AUC %)*			
		IVM	*ANN*	*LR*	*SVM*	*IVM*	*ANN*	*LR*	*SVM*
1	EL, SL, AS, LI, LU	82.57	83.64	82.61	82.18	83.70	83.64	84.29	81.93
2	EL, SL, AS, DF, LU	83.52	85.03	83.35	83.01	85.47	85.03	86.47	83.53
3	EL, SL, CU, LI, LU	82.82	84.17	82.78	82.45	84.50	84.18	85.04	83.11
4	EL, SL, CU, DF, LU	83.77	84.53	83.72	83.19	86.15	84.53	86.83	84.12
5	EL, SL, DD, LI, LU	85.41	86.69	85.30	84.92	85.73	86.69	86.17	85.10
6	EL, SL, LI, DF, LU	82.14	83.59	82.18	81.38	83.55	83.59	84.51	81.61
7	EL, AS, CU, LI, DR	74.99	75.48	74.48	74.10	68.92	75.48	70.40	67.71
8	EL, AS, CU, LI, LU	82.10	82.96	81.99	80.13	81.26	82.96	82.17	79.31
9	EL, AS, CU, DF, DR	75.78	75.70	75.13	74.84	71.85	75.70	73.28	69.78
10	EL, AS, CU, DF, LU	82.77	83.89	82.70	80.22	82.77	83.89	84.14	80.05
11	EL, AS, DD, LI, DR	79.80	81.15	79.34	79.38	74.98	81.15	76.03	74.86
12	EL, AS, DD, LI, LU	84.56	85.93	84.46	83.03	82.98	85.93	83.76	82.77
13	EL, AS, LI, DF, DR	73.80	74.53	73.48	72.97	66.57	74.53	68.06	65.74
14	EL, AS, LI, DF, LU	81.35	82.63	81.57	79.48	80.19	82.63	81.58	77.83
15	EL, CU, DD, LI, DR	79.76	80.75	79.44	79.29	75.71	80.75	76.84	75.57
16	EL, CU, DD, LI, LU	84.50	85.78	84.37	82.70	83.55	85.78	84.33	83.05
17	EL, CU, LI, DF, DR	74.33	75.02	73.96	73.56	68.17	75.02	69.88	68.10
18	EL, CU, LI, DF, LU	81.48	82.69	81.52	79.30	81.18	82.32	82.35	78.70
19	SL, AS, CU, LI, LU	80.93	82.11	80.95	80.34	84.54	82.11	84.83	81.54

NO	*Conditioning factors*	*Training (AUC %)*				*Validation (AUC %)*			
		IVM	*ANN*	*LR*	*SVM*	*IVM*	*ANN*	*LR*	*SVM*
20	SL, AS, CU, DF, LU	81.67	82.88	81.45	80.59	86.09	82.88	86.82	81.99
21	SL, AS, DD, LI, LU	84.18	85.29	84.01	82.80	85.88	85.29	85.92	84.65
22	SL, AS, LI, DF, LU	80.08	81.48	80.10	80.22	83.48	81.48	84.05	81.44
23	SL, CU, DD, LI, LU	84.32	85.06	84.11	82.92	86.35	83.64	86.57	85.12
24	SL, CU, LI, DF, LU	80.71	81.61	80.70	80.26	84.30	81.83	84.78	82.00
25	AS, CU, DD, LI, DR	76.35	77.24	75.82	75.55	74.29	70.82	74.74	72.48
26	AS, CU, DD, LI, LU	83.01	83.37	82.89	81.40	83.47	78.27	83.86	82.12
27	AS, CU, LI, DF, DR	68.44	68.92	67.93	68.21	63.52	63.56	65.11	62.51
28	AS, CU, LI, DF, LU	79.29	80.55	79.36	78.62	80.40	79.19	81.44	79.58
29	EL, SL, AS, CU, LI, LU	83.26	84.65	83.18	82.76	84.24	83.71	84.78	82.62
30	EL, SL, AS, CU, DF, LU	84.20	84.67	83.95	83.63	85.98	80.58	86.83	84.12
31	EL, SL, AS, DD, LI, LU	85.76	87.35	85.62	85.20	85.70	83.14	86.04	84.93
32	EL, SL, AS, LI, DF, LU	82.62	84.18	82.64	82.34	83.35	83.36	84.27	81.98
33	EL, SL, CU, DD, LI, LU	85.77	87.28	85.57	85.23	86.08	84.34	86.51	85.12
34	EL, SL, CU, LI, DF, LU	82.92	83.90	82.89	82.53	84.13	83.88	84.93	82.59
35	EL, AS, CU, DD, LI, DR	80.27	81.89	79.91	79.64	76.09	76.73	77.17	75.93
36	EL, AS, CU, DD, LI, LU	84.91	86.00	84.78	83.57	83.47	80.56	84.21	83.07
37	EL, AS, CU, LI, DF, DR	75.04	76.31	74.70	74.52	68.65	69.65	70.67	68.73
38	EL, AS, CU, LI, DF, LU	82.05	83.45	82.04	80.51	80.97	80.64	82.24	79.58
39	SL, AS, CU, DD, LI, LU	84.62	85.98	84.43	83.17	86.31	83.37	86.42	85.01
40	SL, AS, CU, LI, DF, LU	81.17	82.78	81.16	80.83	84.08	81.61	84.70	81.35

NO	*Conditioning factors*	*Training (AUC %)*				*Validation (AUC %)*			
		IVM	*ANN*	*LR*	*SVM*	*IVM*	*ANN*	*LR*	*SVM*
41	EL, SL, AS, CU, DD, LI, LU	86.05	87.65	85.89	85.63	86.03	85.70	86.40	85.11
42	EL, SL, AS, CU, LI, DF, LU	83.32	84.33	83.25	83.04	83.92	81.77	84.79	83.56

576

577 **Notes**: EL, SL, AS, CU, DD, LI, DF, DR and LU denote conditioning factors of elevation, slope, aspect, curvature, distance to drainage,
578 lithology, distance to fault, distance to road and land use, respectively. IVM, ANN, LR and SVM denote information value model, artificial
579 neural networks, logistic regression, and support vector machine, respectively.

580
581

List of Figure Captions

Figure 1. Landslide inventory map of Chunan, Zhejiang, China.

Figure 2. Correlation between storms and landslides (Note: storm is defined as daily rainfall larger than 50 mm).

Figure 3. Correlation of landslide point density (per 10 km^2) and area percentage of various conditioning factors.

Figure 4. Map of geologic units.

Figure 5. Variation of AUC in model (a) training and (b) validation in applying IVM, LR, ANN and SVM under the changing of conditioning factors and prediction rate curve (c) of the optimum model.

Figure 6. Variation of area percentage of classified (a) very low, (b) low, (c) moderate and (d) high hazard zones applying IVM, LR, ANN and SVM under the changing of conditioning factors.

Figure 7. Landslide hazard zone maps produced by (a) IVM, (b) LR, (c) ANN and (d) SVM.

Figure 8. Statistics and spatial patterns of landslide susceptibility maps produced by IVM , LR, ANN and SVM (Note: VL, L, M, and H denote the hazard levels of very low, low, moderate and high, respectively).

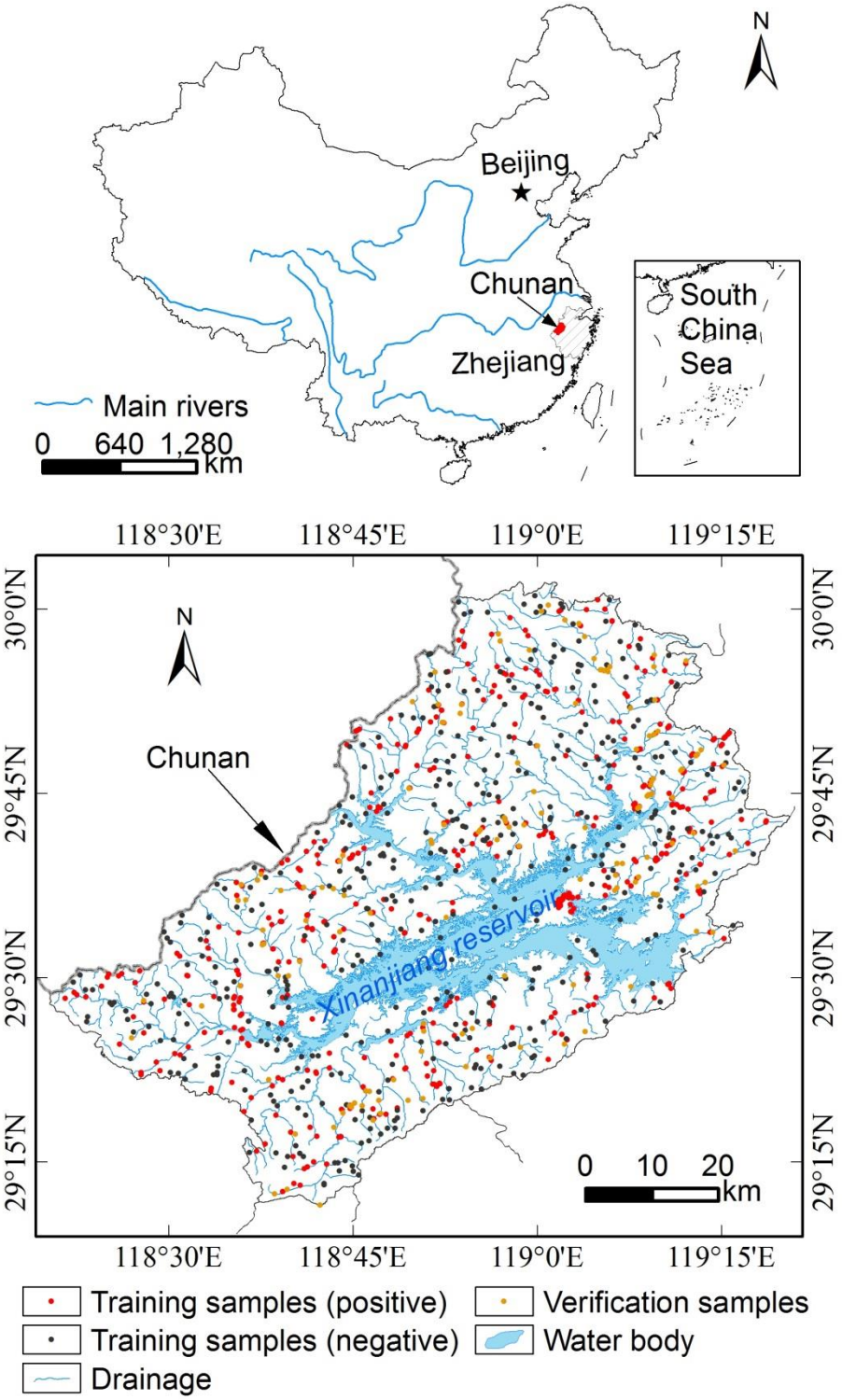

Figure 1. Landslide inventory map of Chunan, Zhejiang, China.

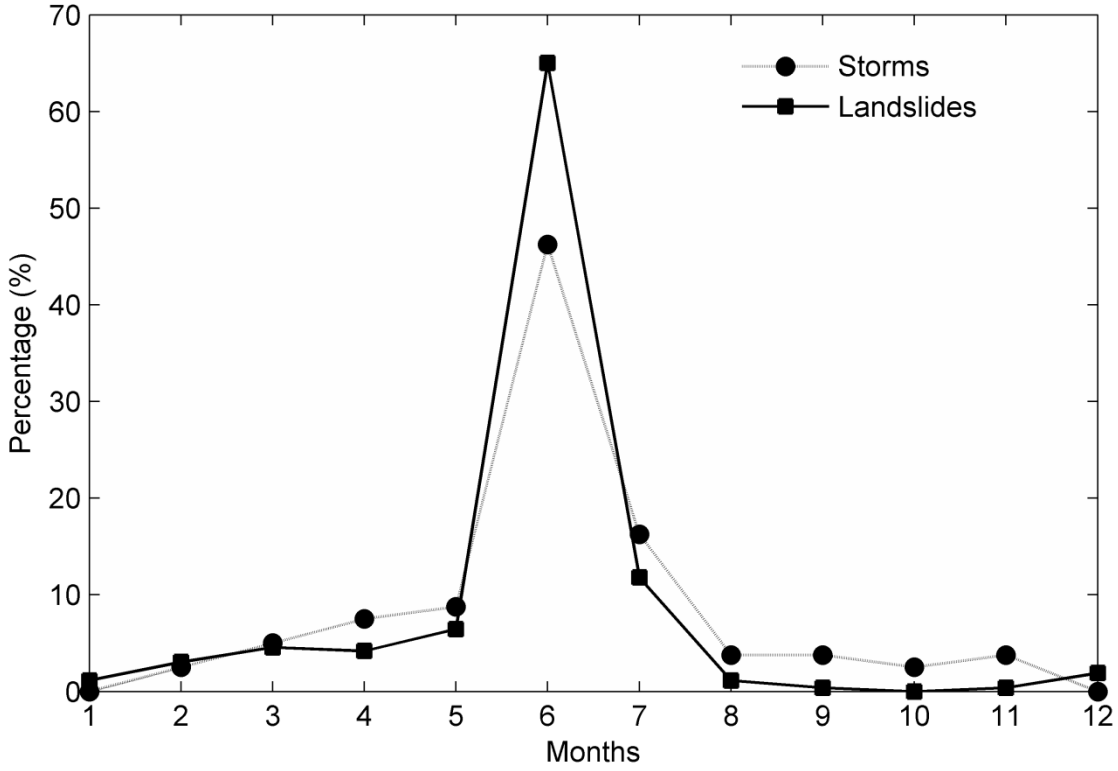

Figure 2. Correlation between storms and landslides (Note: storm is defined as daily rainfall larger than 50 mm).

609

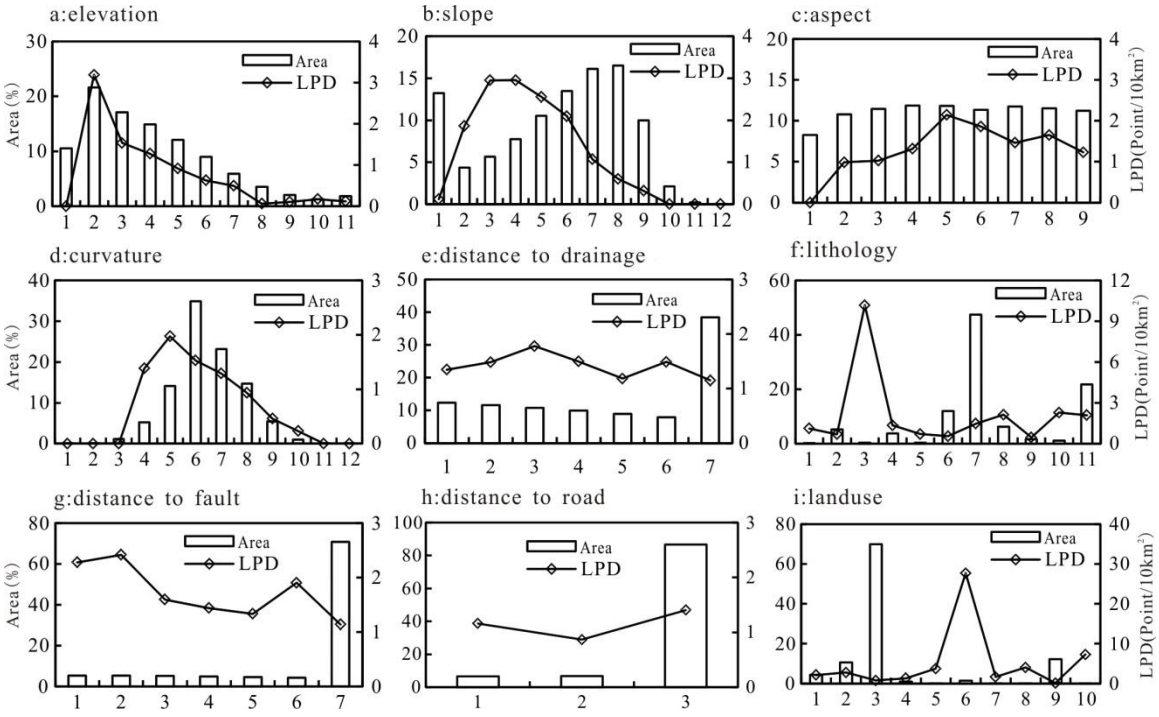

610

611 **Figure 3.** Correlation of landslide point density (per 10 km^2) and area percentage of

612 various conditioning factors.

613

614

615

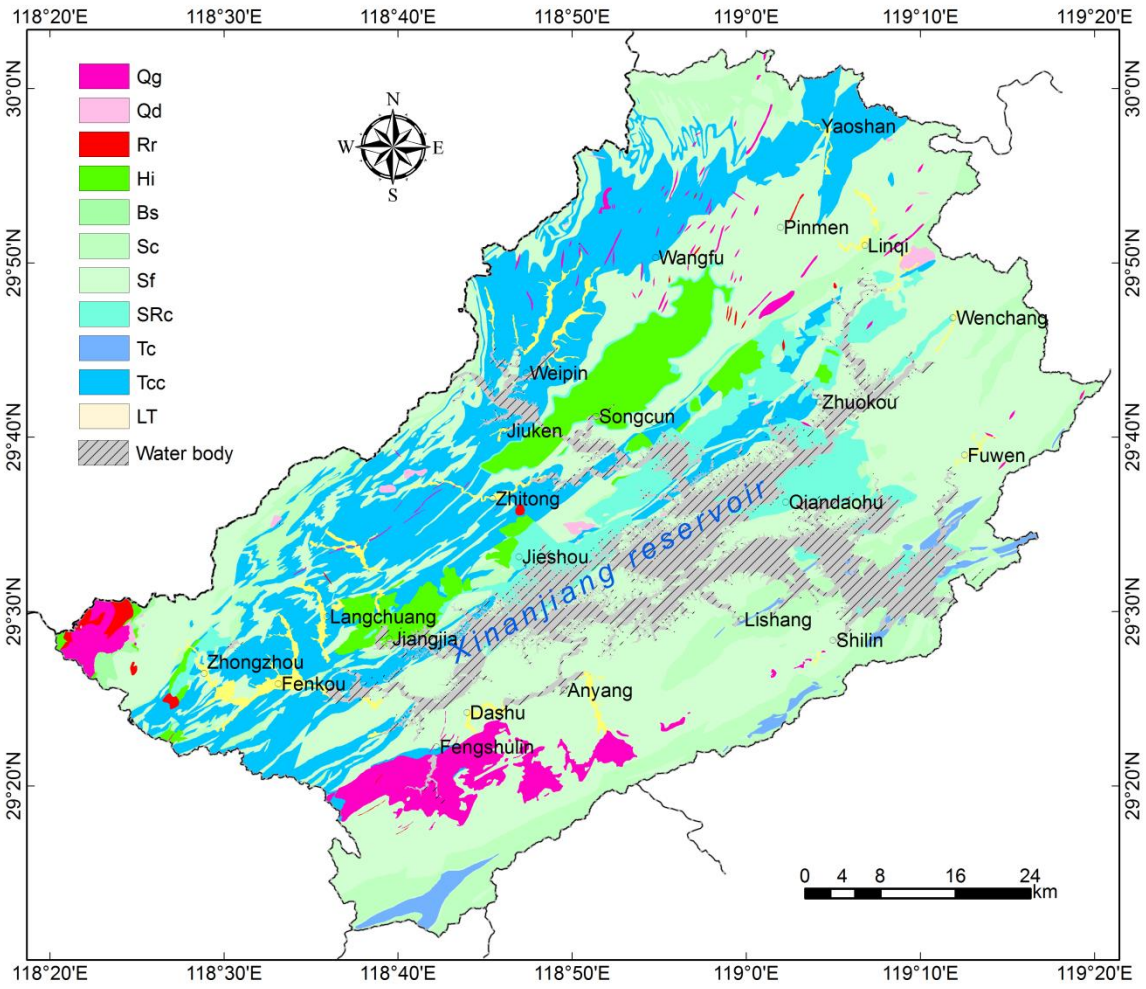

Figure 4. Map of geologic units.

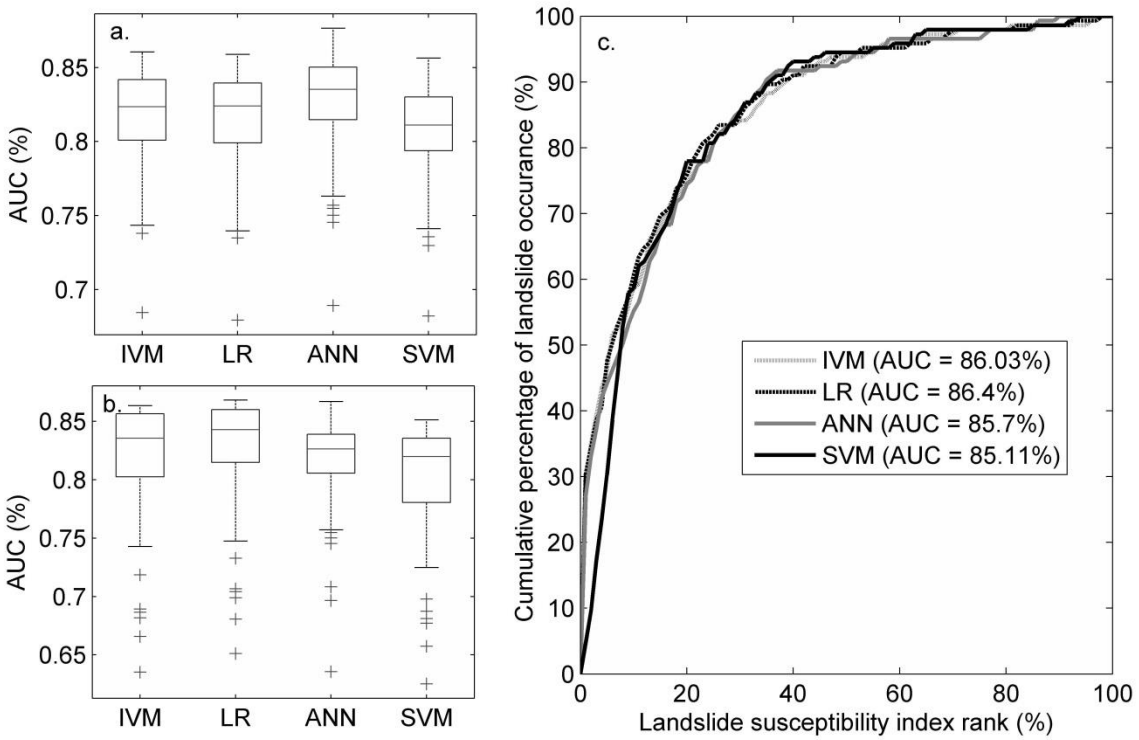

620

621 **Figure 5.** Variation of AUC in model (a) training and (b) validation in applying IVM, LR,
622 ANN and SVM under the changing of conditioning factors and prediction rate curve (c)
623 of the optimum model.

624

625

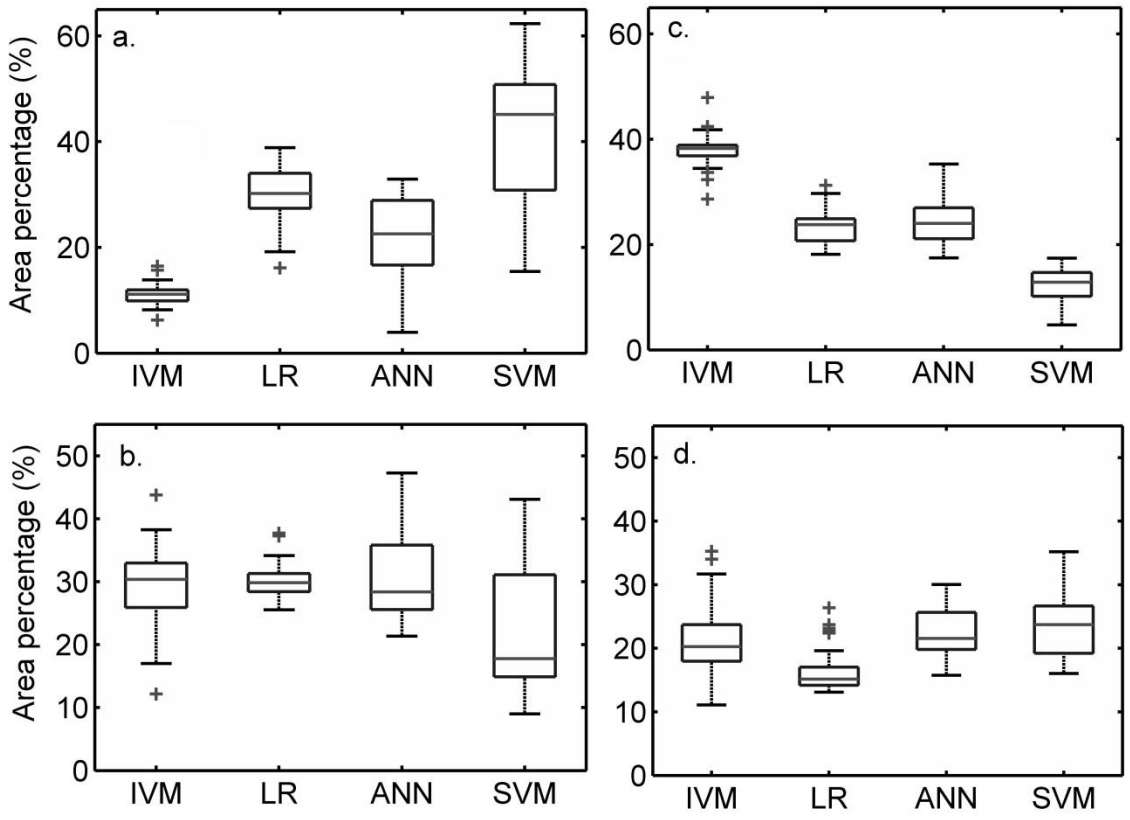

626

627 **Figure 6.** Variation of area percentage of classified (a) very low, (b) low, (c) moderate
628 and (d) high hazard zones applying IVM, LR, ANN and SVM under the changing of
629 conditioning factors.

630

631

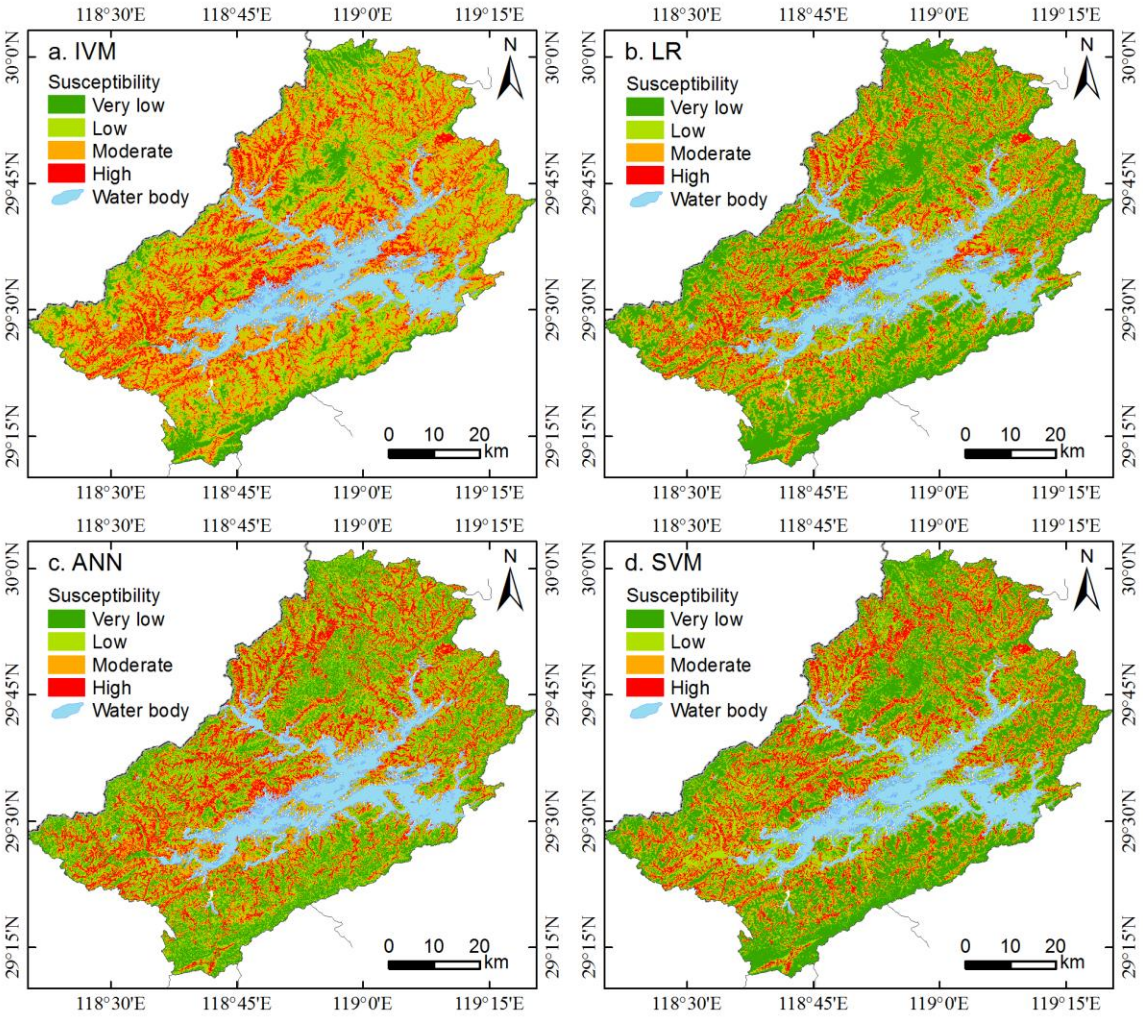

632

633 **Figure 7.** Landslide hazard zone maps produced by (a) IVM, (b) LR, (c) ANN and (d)
634 SVM.

635

636

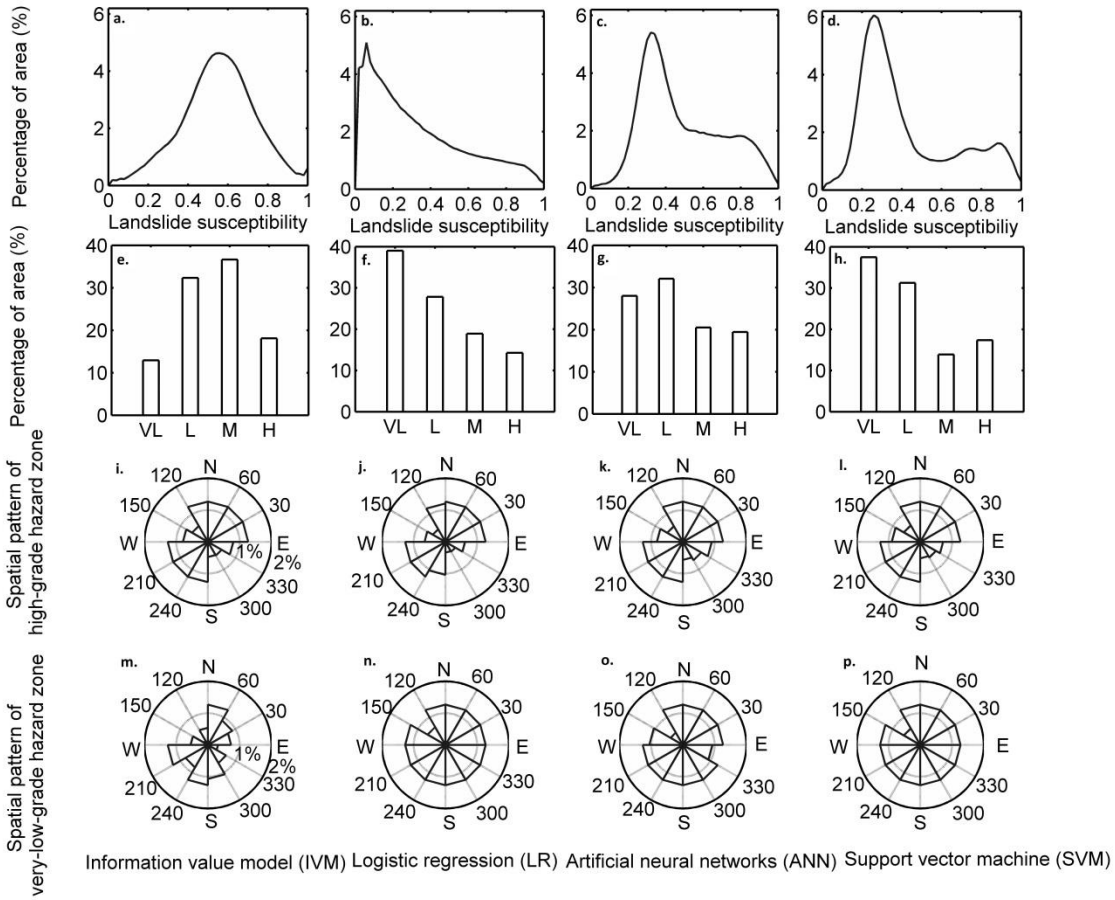

637

638 **Figure 8.** Statistics and spatial patterns of landslide susceptibility maps produced by
639 IVM , LR, ANN and SVM (Note: VL, L, M, and H denote the hazard levels of very low,
640 low, moderate and high, respectively).

641